

# Effects of Surfactant and Boron Doping on the BWF Feature in the Raman Spectrum of Single-Wall Carbon Nanotube Aqueous Dispersions<sup>†</sup>

Jeff L. Blackburn,\* Chaiwat Engtrakul, Timothy J. McDonald, Anne C. Dillon, and Michael J. Heben

Center for Basic Science, National Renewable Energy Laboratory, Golden, Colorado 80401

Received: August 15, 2006; In Final Form: September 27, 2006

We examine the Breit–Wigner–Fano (BWF) line shape in the Raman spectra of carbon single-wall nanotubes (SWNTs) dispersed in aqueous suspensions. Bundling and electronic effects are studied by comparing undoped SWNTs (C-SWNTs) to boron-doped nanotubes (B-SWNTs) in a variety of different surfactant solutions. For SWNTs dispersed with nonionic surfactants that are less effective in debundling than ionic surfactants, the Raman spectra retain a large BWF feature. However, we demonstrate that even for SWNTs dispersed as isolated nanotubes by ionic surfactants the BWF feature may be present and that the intensity of the BWF is highly sensitive to the specific surfactant. In particular, surfactants with electron-donating groups tend to enhance the BWF feature. Also, modification of the SWNT electronic properties by boron doping leads to enhanced surfactant dispersion relative to undoped C-SWNTs and also to modification of the BWF feature. These observations are in agreement with reports demonstrating an enhancement of the BWF by bundling but also agree with reports that suggest electron donation can enhance the BWF feature even for isolated SWNTs. Importantly, these results serve to caution against using the lack or presence of a BWF feature as an independent measure of SWNT aggregation in surfactant dispersions.

## Introduction

Carbon single-wall nanotubes (SWNTs) are unique one-dimensional materials with optical, electronic, and vibrational properties that are dependent on the nanotube diameter and chiral angle. The tunable electronic properties of SWNTs make them ideal candidates for a variety of applications including field-effect transistors,<sup>1,2</sup> chemical sensors,<sup>3</sup> photovoltaic (PV) materials,<sup>4,5</sup> organic light-emitting diodes (OLEDs),<sup>6</sup> and energy storage media.<sup>7,8</sup> As produced, SWNT samples consist of a ~2:1 mixture of semiconducting and metallic nanotubes (s-SWNTs and m-SWNTs, respectively) of various band gaps and exist in bundles of varying size because of strong intertube van der Waals forces.<sup>9</sup> This presents a challenge for the incorporation of SWNTs into devices, because each different device may perform ideally with a specific nanotube type or band gap. These requirements underscore the importance of producing homogeneous dispersions of isolated SWNTs and of finding methods for separating SWNTs according to diameter and helicity. It is also important to probe the interaction of SWNTs with other molecules and to understand the effect of this interaction on device performance. For example, the change in electrical conductance upon molecular adsorption is the primary mechanism by which SWNTs sense chemicals.<sup>3</sup> Also, both static and dynamic charge transfer in SWNT/polymer composites are important for energy storage or energy conversion devices.<sup>10–12</sup>

Raman spectroscopy is an especially powerful tool for characterization of SWNTs.<sup>13,14</sup> Raman spectroscopy has been used to glean information on the degree of SWNT debundling and isolation,<sup>15–18</sup> the relative contents of s-SWNTs and m-SWNTs in a given sample,<sup>19,20</sup> and the electronic redistribution or charge transfer as a function of molecular interactions.<sup>21</sup>

Raman measurements are particularly sensitive to m-SWNTs, relative to other spectroscopic techniques, as m-SWNTs cannot be observed with PLE spectroscopy and are difficult to interrogate by absorbance spectroscopy in polydisperse distributions. This sensitivity is due in part to the appearance of a broadened, asymmetric peak with a Breit–Wigner–Fano (BWF) line shape in the Raman spectrum of m-SWNTs that arises from coupling of the  $A_{1g}$  phonon to the electronic continuum. The region of the Raman spectrum specific to atomic displacements tangential to the tube surface (tangential or G-band region) is actually composed of two peaks for m-SWNTs. The  $G^+$  mode at  $\sim 1580\text{ cm}^{-1}$  is due to displacements along the tube axis, and the diameter-dependent  $G^-$  mode between  $\sim 1530$  and  $1560\text{ cm}^{-1}$  is due to displacements along the tube circumference.<sup>13</sup> Brown et al. showed that nanotube curvature was responsible for both the frequency difference between the two components as well as the coupling of the lower frequency  $G^-$  mode to the conduction electron continuum.<sup>22</sup> The BWF line shape is described by

$$I(\omega) = I_0 \frac{[1 + (\omega - \omega_{\text{BWF}})/q\Gamma]^2}{1 + [(\omega - \omega_{\text{BWF}})/\Gamma]^2}$$

where  $1/q$  is a parameter which measures the interaction of the phonon with a continuum of states,  $\omega_{\text{BWF}}$  is the BWF frequency at maximum intensity  $I_0$ , and  $\Gamma$  is the broadening parameter.<sup>23</sup>

The origin of the BWF component, as well as the sensitivity of the BWF component to a variety of intrinsic and extrinsic factors, has been the subject of much recent debate. Initial reports suggested that the BWF component was intrinsic to individual m-SWNTs, arising from the coupling of the discrete  $A_{1g}$  phonon to the continuum of electrons at the Fermi level in the m-SWNTs.<sup>22,24</sup> Consistently, early reports demonstrated the

<sup>†</sup> Part of the special issue “Arthur J. Nozik Festschrift”.

\* Author to whom correspondence should be addressed.

presence of a BWF line shape for m-SWNTs isolated on substrates.<sup>24</sup> However, more recent reports call these findings into question by demonstrating the lack of this mode for m-SWNTs isolated on substrates.<sup>25,26</sup> These latter experiments support a competing idea that the BWF coupling arises from low frequency, gapless plasmon modes in the far-infrared that are strongly enhanced by bundle formation.<sup>27</sup> Other recent reports correlating the BWF intensity with temperature and X-ray diffraction data also claim an enhancement because of bundling, although these experiments were not done with single-tube resolution.<sup>28,29</sup>

The dispersion of SWNTs in aqueous solution with surfactants<sup>30</sup> and polymers<sup>31</sup> represents a crucial advancement toward providing debundled, isolated nanotubes that are easily processed for device fabrication. The degree of debundling in SWNT solutions has been assessed by PLE, absorbance, and Raman spectroscopy. Raman experiments performed on SWNTs dispersed in aqueous solution with sodium dodecyl sulfate (SDS), single-stranded DNA, polyvinylphenol (PVP), and aragoza polymers demonstrated the disappearance of the BWF line shape once the SWNTs were isolated in solution.<sup>16,17</sup> In general, the appearance and disappearance of the BWF was attributed to bundling/debundling effects, in similarity to studies performed on SWNTs isolated on substrates. Following this reasoning, Karachevtsev et al. used the ratio of the higher frequency  $G^+$  component to the BWF component ( $G^+/G^-$ ) as a measure to compare the relative degree of SWNT aggregation in different surfactant and polymer suspensions and films.<sup>17</sup>

However, in addition to the bundling effect, the BWF component has also been shown to exhibit sensitivity to electron donation and withdrawal from m-SWNTs. For example, SWNT oxidation by acidic species such as  $HNO_3$ ,  $H_2SO_4$ , and Nafion has been shown to cause a diminishment of the BWF feature.<sup>32–34</sup> Strano et al. also studied SDS-suspended HipCo SWNTs with a large BWF component at basic pH and observed a downshift and narrowing of this feature with decreasing pH.<sup>35</sup> In these cases, the proton localizes fractional charge at the nanotube surface at low pH, leaving a net positive charge ( $\delta^+$ ) over the remainder of the nanotube. Shim et al. showed that, while the BWF mode was absent for substrate-suspended isolated SWNTs, the adsorption of the electron-donating polymer polyethyleneimine (PEI) induced a large BWF component for the isolated SWNTs.<sup>11</sup> The enhancement of the BWF feature for m-SWNTs has been shown upon n-type doping with Li,<sup>36</sup> and the development of a BWF feature for s-SWNTs was shown for doping with Cs, Rb, and K.<sup>21,37</sup> These latter examples demonstrate an enhancement of the BWF feature when injected electronic charge ( $\delta^-$ ) is delocalized over the length of the nanotubes. In general, these reports demonstrate the tendency for diminishment of the BWF feature when electron density is withdrawn from m-SWNTs, while the BWF feature is strengthened when electron density is donated to m-SWNTs. These results suggest a strong dependence of the BWF mode on the localization or polarization of charge on the nanotube surface induced by molecular interactions, even for completely debundled SWNTs. Clearly, these results suggest that caution must be taken in attributing changes in BWF intensity solely to the degree of SWNT aggregation and emphasize the need for further studies.

In this contribution, we examine the role of bundling and nanotube–surfactant interactions on the BWF Raman component for dispersions of SWNTs in various surfactants. Interestingly, we find that the intensity of the BWF component is sensitive to both the degree of debundling and the differences

in the SWNT–surfactant interactions, both of which lead to varying degrees of charge localization at the nanotube surface. In several cases, we observe a strong BWF component in the metallic Raman spectrum even for dispersions of highly isolated SWNTs. The intensity of the BWF mode tends to be higher for surfactants containing electron-donating groups, suggesting that charge injection may contribute to the BWF feature in dispersions of isolated SWNTs. This hypothesis is supported by the observation that modifications in the electronic distribution induced by boron doping also lead to significant differences in the BWF intensity for nanotubes dispersed with a given surfactant. In general, our results, coupled with results from the literature, suggest that the presence and intensity of the BWF feature is sensitive to any changes in the magnitude of dielectric screening, whether from tube–tube interactions in bundles, from charge injection or depletion, or from charge polarization from tube–molecule interactions. These results suggest that the existence or lack of a BWF feature should not be used alone as a measure of SWNT aggregation and also provide information regarding the nature of surfactant–nanotube interactions.

## Experimental Section

SWNTs were produced by laser vaporization of a graphite target containing the appropriate catalysts. C-SWNTs were produced from graphite targets having 0.6 atomic % each of Ni and Co powder. Boron-doped SWNTs were produced from graphite targets containing 11 atomic % nickel boride (NiB). Boron is doped substitutionally into the lattice of these B-SWNTs at a level of  $\sim 1$ –1.5 atomic % relative to carbon.<sup>38</sup> Targets were made by pressing 5 g of material at 10 000 psi in a cylindrical die 1-in. in diameter. Targets are mounted in a molybdenum holder and positioned into a quartz tube surrounded by a clamshell furnace. The furnace temperature during synthesis was 1175 °C. Nitrogen was used as the background gas at a pressure of 500 Torr and at a flow rate of 100 cm<sup>3</sup>/min. Samples were vaporized with a pulsed alexandrite laser, running in the free mode at 10 Hz, which produces 755 nm pulses which are  $\sim 200$  ns in duration. Laser power ranged from 2 to 4 W at power densities of 45–65 W/cm<sup>2</sup> to remain in a vaporization regime.<sup>39,40</sup> Material was produced at a rate of  $\sim 30$  mg/h and was collected in the cold zone downstream of the furnace.

To study a variety of samples, we also synthesized C-SWNTs and B-SWNTs using a Nd:YAG laser and C-SWNTs using arc discharge. Although this report focuses on SWNTs produced with the alexandrite laser, the same trends are seen for SWNTs generated with the Nd:YAG laser and arc discharge.

Surfactant dispersions of SWNTs were prepared in a manner similar to that described previously.<sup>30,41</sup> Sodium dodecyl sulfate (SDS), sodium dodecyl benzyl sulfonate (SDBS), sodium cholate (cholate), and Tween 80 were purchased from Aldrich and were used without further purification. Triton X-100 was purchased from EMD and was used without further purification. Figure 1 displays the chemical structures of several of the surfactants utilized in this study. Briefly, 6–10 mg of SWNT raw soot was added to 15 mL of a 1% (by weight) D<sub>2</sub>O solution of a given surfactant. This dispersion was sonicated with a cup-horn sonicator at 30% power for 12 min and then was transferred to a bath sonicator for 24 h. Following bath sonication, the dispersion was again sonicated with the cup-horn sonicator, this time at 100% power for 12 min. The dispersions were then immediately centrifuged at 28 000 rpm for 4 h at 20 °C. The supernatant was carefully removed via pipet for use in absorbance and Raman measurements.

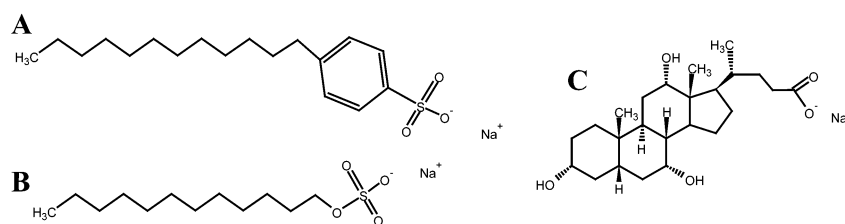


**Figure 1.** Chemical structures of the anionic surfactants used in this study. (A) sodium dodecyl benzyl sulfonate (SDBS), (B) sodium dodecyl sulfate (SDS), and (C) sodium cholate (cholate).

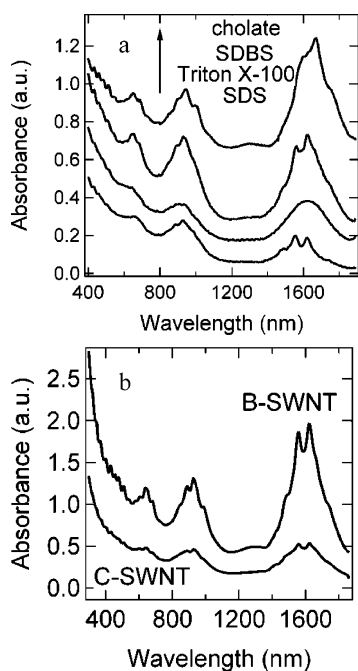


**Figure 2.** (a) Absorbance spectra of C-SWNTs dispersed with four different surfactants. Spectra are not normalized but are offset for clarity. (b) Un-normalized absorbance spectra for B-SWNTs and C-SWNTs dispersed in 1 wt % SDBS/D<sub>2</sub>O solution. The starting mass of raw material for each sample was 9 mg, and all absorbance spectra were taken in 1-cm cuvettes.

Steady-state absorbance measurements were made using a Cary 500 double beam spectrometer at a spectral resolution of 1 nm. Absorbance and Raman spectra were recorded for solutions in 1-cm cuvettes. Raman measurements were made with an argon ion laser (488 nm, 2.54 eV excitation) or a helium neon laser (633 nm, 1.96 eV excitation) in the back-scattering configuration. Because excitation at 633 nm is specific for m-SWNTs in the diameter range for these samples (1.2–1.5 nm, *vide infra*), only data for 633-nm excitation are displayed and discussed in this report. For dry samples and films, the excitation power was kept below 5 mW to avoid sample heating. Because of the high heat capacity of water, sample heating for the SWNT suspensions was not a problem. Up to the highest power used, 22 mW at 633-nm excitation wavelength, no shifts in any Raman peak positions or relative intensities were observed and the Stokes/anti-Stokes ratios remained constant. Thus, the power was adjusted to provide good signal to noise for each suspension on the basis of the optical density of the solution.

## Results

Figure 2 shows the absorbance spectra for several of the solutions examined in this study. Figure 2a shows undoped

C-SWNTs dispersed in cholate, SDBS, Triton X-100, and SDS. Individual peaks in the absorbance spectra arise from optically induced transitions between van Hove singularities (vHs) in the density of states (DOS) for SWNTs of specific chiralities. Three main groupings of peaks may be seen in the absorbance spectra: (1) peaks from ~1400 to 1900 nm arising from the first vHs transitions for s-SWNTs, (2) peaks from ~800 to 1100 nm arising from the second vHs transitions for s-SWNTs, and (3) peaks from ~580 to 780 nm arising from the first vHs transitions for m-SWNTs. The structure at wavelengths shorter than ~580 nm arises from the third optical transitions for s-SWNTs, which are superimposed on a rising background.

The absorbance spectra for the nonionic Triton X-100 sample and the Tween 80 sample (not shown) are broad and relatively featureless compared to the spectra of the SWNTs dispersed in anionic surfactants. This observation, coupled with the lack of photoluminescence (PL, not shown) from these samples, suggests poor debundling for these nonionic surfactants. In contrast, the anionic surfactants debundle the SWNTs relatively effectively, as evidenced by well-resolved peaks in the absorbance spectrum as well as significant and well-resolved PL. In agreement with previous studies, we see a dependence of the SWNT peak positions in absorbance and PL on the dielectric environment of the solution, which is determined by the surfactant.<sup>42</sup> For the anionic surfactants, we find the best dispersion of these laser-generated SWNTs is achieved with cholate, followed by SDBS, and then SDS.<sup>41,42</sup> This is likely a reflection of the strength of the surfactant–nanotube interactions.<sup>41,43,44</sup>

Figure 2b shows absorbance spectra for boron-doped SWNTs (B-SWNTs) and C-SWNTs, both dispersed in 1% SDBS/D<sub>2</sub>O solution. The carefully analyzed second derivatives of the absorbance spectra (not shown), as well as PLE peak positions, demonstrate that boron doping does not induce any changes in the peak positions of s- or m-SWNTs. This suggests that the characteristic electronic structure of the SWNTs is maintained at these low doping levels and that the optical properties are still defined by the transitions between the one-dimensional van Hove singularities. As evidenced by the higher optical density of the B-SWNT solution, these ~1% doped B-SWNTs show remarkably enhanced dispersion in surfactant solutions compared to undoped C-SWNTs, suggesting reduced intertube van der Waals forces and enhanced tube–surfactant interactions. This result is found for every surfactant utilized in this study except for cholate which, surprisingly, does not suspend the B-SWNTs at all. This effect will be discussed in detail in subsequent portions of this manuscript.

Figure 3 displays the radial breathing mode (RBM) region of the spectrum for several samples. The RBMs are slightly upshifted relative to the dry sample<sup>45</sup> and are in the range of ~160–190 cm<sup>-1</sup>, indicating a diameter range of ~1.2–1.5 nm.<sup>46</sup> Excitation at 633 nm for this diameter range is in resonance with the first vHs transitions for several m-SWNTs.

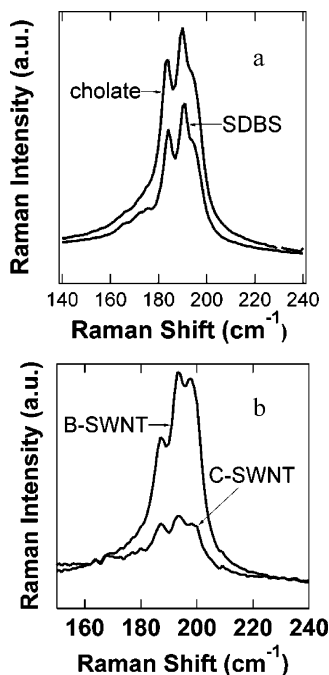


**Figure 3.** RBM Raman spectra, excited at 633 nm for several dispersions discussed in this report. (a) C-SWNTs dispersed in SDBS and cholate. (b) B-SWNTs and C-SWNTs dispersed in SDBS.

Possible m-SWNT species which may be resonant with 633 nm in our sample include the (16,1), (11,8), (12,6), (9,9), and (13,4) SWNTs. Analysis of the G-band spectra, discussed below, demonstrates that some s-SWNTs are also probed at this wavelength, likely because of resonance with the third optical transitions for a small number of s-SWNTs. From Figure 3b, we consistently observe enhanced intensity of the RBMs for B-SWNTs, an effect that was also reported earlier for laser-generated B-SWNTs.<sup>47</sup> In this study, the authors posited that the enhancement was due to a shifting of the optical transitions by a few meV, while our analysis of absorbance and PLE data suggest that the positions of the optical transitions do not change as a result of boron doping. We believe that the enhancement may result from an enhancement of the absorbance cross section induced by substitutional boron doping.<sup>48</sup>

To study a variety of samples, we also synthesized and dispersed undoped C-SWNTs using a Nd:YAG laser and an arc discharge technique as well as B-SWNTs with the Nd:YAG laser. The samples made with the Nd:YAG laser and with arc discharge have RBMs in the range of  $\sim 180\text{--}210\text{ cm}^{-1}$ , indicating a slightly smaller mean diameter than the SWNTs prepared with the alexandrite laser.

Figure 4 compares the G-band Raman spectrum of the unpurified, dry C-SWNT sample to the spectra of the same SWNTs in a variety of surfactant dispersions. The Raman spectrum for the dry sample is a convolution of several peaks corresponding to both semiconducting and metallic SWNTs.<sup>22,49,50</sup> Specifically, it has been shown that s-SWNTs display four peaks in this region at  $\sim 1607$ , 1592, 1569, and  $1553\text{ cm}^{-1}$ ,<sup>50</sup> while the spectrum for m-SWNTs may be fit with one Lorentzian at  $\sim 1580\text{ cm}^{-1}$  and a BWF feature in the region of  $\sim 1530\text{--}1560\text{ cm}^{-1}$ .<sup>22</sup> The G-band spectrum for the dry sample is fit well with six components with frequencies near these values. The peak at  $\sim 1535\text{ cm}^{-1}$  is asymmetric and returns slowly to the baseline at low energy and is fit best with a BWF line shape with  $1/q = -0.13$  and  $\Gamma = 30\text{ cm}^{-1}$ . These same parameters were used as first approximations in the fitting of all other spectra, and values near these initial guesses resulted in good fits.

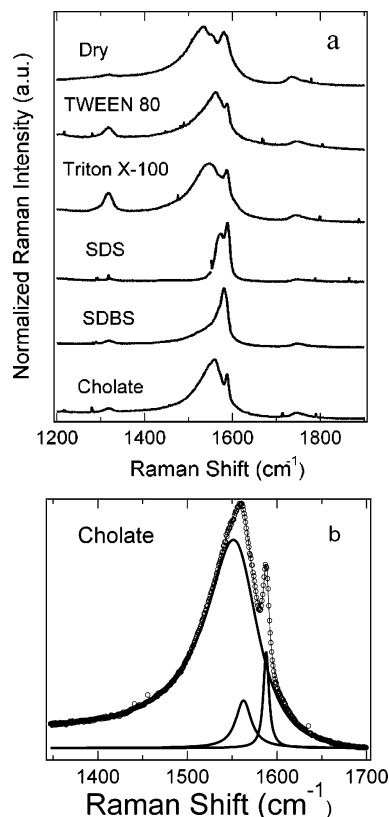


**Figure 4.** (a) Raman spectra excited at 633 nm of C-SWNTs in dry, powder form and dispersed in D<sub>2</sub>O with various surfactants. Spectra are normalized and offset for clarity. (b) Demonstration of fitting for Raman spectrum of C-SWNT sample dispersed with cholate. Data (points) are fit with two Lorentzians and one BWF line shape (dark lines) to give composite fit (thin solid line). Fitting parameters are given in Table 1.

The G-band spectra for the C-SWNT dispersions are significantly different from the spectrum of the dry sample. The spectrum for the TWEEN-dispersed SWNTs shows contributions mainly from the  $1589\text{ cm}^{-1}$  semiconducting peak and a large BWF component at  $\sim 1550\text{ cm}^{-1}$ . An intense BWF peak is also observed for the Triton X-100 sample. For the SDBS-dispersed sample, the intensity of the BWF mode is dramatically reduced relative to the TWEEN and Triton samples, and the BWF is completely absent for the SDS-dispersed sample. Finally, for the cholate sample, a very strong BWF feature is observed, an interesting observation given the fact that this surfactant produces highly debundled, isolated SWNTs. The fitting parameters for the spectra of C-SWNTs in the three different anionic surfactants are listed in Table 1.

To further explore electronic effects and the effect of tube-surfactant interactions, we also compared the dry and solution-phase Raman spectra of B-SWNTs to the undoped C-SWNTs. Figure 5 compares the Raman spectra for B-SWNTs and C-SWNTs in dry form and in dispersions with Triton X-100, SDBS, and SDS. The fitting parameters for the spectra of B-SWNTs in SDS and SDBS are listed in Table 1. In the dry form, the spectra look fairly similar, with a slightly diminished BWF intensity in the B-SWNT spectrum. A diminishment in BWF intensity for a dry B-SWNT sample was also seen, although not commented on, in a previous report on laser-generated B-SWNTs (Figure 5a, ref 47). In the dispersions, the relative intensities of the various tangential modes are altered to varying degrees by the substitutional doping of boron into the SWNT lattice. In the Triton X-100 surfactant (Figure 5b),

**TABLE 1: Fitting Parameters for the Raman Spectra of C-SWNTs and B-SWNTs in Anionic Surfactant Solutions<sup>a</sup>**

sample	surfactant	$\omega$ (cm <sup>-1</sup> )	$\Gamma$ (cm <sup>-1</sup> )	$1/q$	$G^-/G^+$
C-SWNT	SDS	1565 <sup>S</sup>	15		
		1575 <sup>M</sup>	16		
		1589 <sup>S</sup>	11		
	SDBS	1548 <sup>M</sup>	32	-0.32	0.6
		1567 <sup>S</sup>	27		
		1582 <sup>M</sup>	17		
		1557 <sup>M</sup>	35	-0.16	6.9
cholate	1563 <sup>S</sup>	21			
	1588 <sup>S</sup>	8			
	1563 <sup>S</sup>	20			
	1574 <sup>M</sup>	15			
	1588 <sup>S</sup>	11			
B-SWNT	SDS	1563 <sup>S</sup>	20		
		1574 <sup>M</sup>	15		
		1588 <sup>S</sup>	11		
	SDBS	1557 <sup>M</sup>	46	-0.22	4.0
		1559 <sup>S</sup>	14		
		1566 <sup>S</sup>	18		
		1578 <sup>M</sup>	18		
1588 <sup>S</sup>	8				

<sup>a</sup> The frequencies ( $\omega$ ) and FWHM ( $\Gamma$ ) are listed for the Lorentzian features, while additionally the ( $1/q$ ) value is given for the BWF features. S and M label peaks corresponding to semiconducting and metallic SWNTs, respectively, as inferred from ref 22. The  $G^-/G^+$  ratio is the ratio of the area of the BWF ( $G^-$ ) to all other Lorentzian components of the fits.

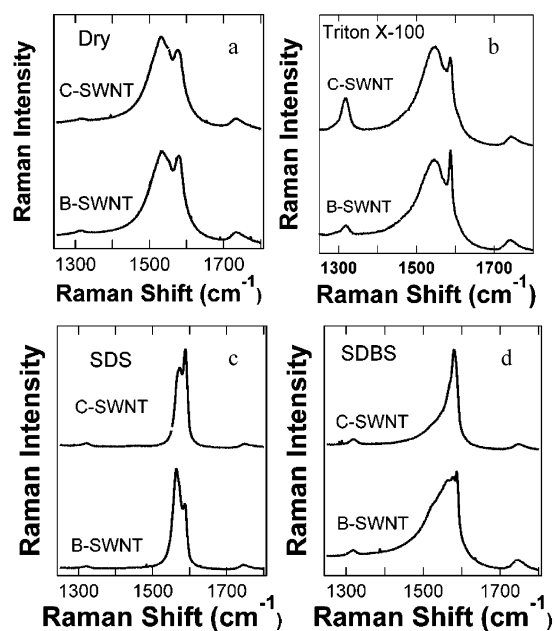


**Figure 5.** Comparison of Raman spectra, excited at 633 nm, for B-SWNTs and C-SWNTs in (a) the dry form and dispersed with three surfactants: (b) Triton X-100, (c) SDS, and (d) SDBS. Spectra are normalized and offset for clarity.

both spectra are dominated by the semiconducting peak around 1588 cm<sup>-1</sup> and a large BWF feature peaking around 1545 cm<sup>-1</sup>.

Interestingly, the same peaks are seen for C-SWNTs and B-SWNTs dispersed in SDS (Figure 5c), but the relative intensities differ. No BWF feature is present in the spectrum for either SDS-dispersed sample. For the SDBS-suspended B-SWNT sample (Figure 5d), several changes are seen relative to the C-SWNT sample. The B-SWNT spectrum contains two semiconducting peaks that are not present in the SDBS-dispersed C-SWNT sample, and the relative intensity of the BWF is greatly enhanced ( $G^-/G^+$  ratio, Table 1). No significant shifts in the frequencies of any of the G-band peaks, within our experimental resolution, are seen in the dry or dispersed samples as a result of boron doping.

We finally comment on the interesting observation that several variations occur for the semiconducting peaks as a function of surfactant and boron doping. For example, the  $\sim 1588$  cm<sup>-1</sup> semiconducting peak is prominent in the SDS and cholate C-SWNT spectra but is absent in the SDBS C-SWNT spectrum (Figure 4a, Table 1). Also, the  $\sim 1563$  cm<sup>-1</sup> semiconducting peak is enhanced for the B-SWNTs relative to the C-SWNTs dispersed in SDS (Figure 5c, Table 1), and the B-SWNT spectrum contains two semiconducting peaks that are not present in the SDBS-dispersed C-SWNT sample. These effects warrant their own study, and we are currently pursuing a multiwavelength Raman study in which we correlate variations in the Raman semiconducting peaks to changes in photoluminescence and absorbance. These results will be reported at a later date. For conciseness and clarity, we discuss changes in only the BWF feature in this report.

## Discussion

It is remarkable that such large variations in the relative ratios of the tangential modes, the BWF in particular, are seen as a function of surfactant. To understand these variations, we consider the effects of bundling, the Raman resonance conditions, pH effects, nanotube–surfactant interactions, and boron doping.

**Bundling.** The absorption transitions of SWNTs are broadened by proximity with other nanotubes, and the PL from semiconducting SWNTs is quenched via contact with co-bundled metallic SWNTs. Thus, the broad, featureless absorbance spectra and lack of PL for SWNTs dispersed with Tween 80 and Triton X-100 suggest that the SWNTs remaining in solution after ultracentrifugation are at least lightly bundled and do not exist as well-isolated nanotubes. On the contrary, well-resolved peaks corresponding to interband transitions for individual SWNT species are observed in the absorbance and PLE spectra for SWNTs dispersed in the anionic surfactants. Islam et al. showed, by AFM, that HipCo SWNTs sonicated in SDBS, without ultracentrifugation, contained  $\sim 74 \pm 5\%$  isolated tubes, with the remaining tubes being bundled.<sup>44</sup> This number was even higher,  $90 \pm 5\%$ , for laser-generated SWNTs, similar to those SWNTs studied here. This implies that the ultracentrifuged samples should contain predominantly isolated SWNTs encased in surfactant micelles, while a contribution from a small percentage of narrow bundles may also exist. The percentage of isolated tubes was much lower for SDS,  $16 \pm 2\%$ ,<sup>44</sup> in agreement with other studies that have found higher dispersion yields and better-resolved absorbance and PLE spectral features for SDBS (relative to SDS) with ultracentrifugation.<sup>41,42</sup> These reports<sup>41,42</sup> also found the highest dispersion yields for the cholate surfactant, in complete agreement with our absorbance and PLE data, which suggest the dispersion yields follow the pattern cholate > SDBS > SDS. These dispersion yields suggest that the highest fraction of isolated, debundled SWNTs exist in the SWNT–cholate sample.

At first inspection, the presence of an intense BWF component for the poorly debundled TWEEN 80 and Triton X-100 samples and the lack of this feature for the SDS sample seems to support the assertion that the BWF intensity is strongly dependent on the degree of SWNT aggregation.<sup>25,26</sup> This assertion is challenged, however, by the observation of BWF components in the spectra for the SDBS- and cholate-suspended samples. In fact, the shape, position, and intensity of the BWF feature are almost identical for the SWNTs suspended in cholate and in TWEEN, and the feature is actually slightly more intense for the cholate sample relative to the TWEEN sample. This is

surprising, given the fact that the cholate surfactant debundles SWNTs very effectively, while TWEEN produces samples with a very low degree of SWNT isolation. Also, among the anionic surfactants that produce well-isolated SWNTs, the BWF intensity is the highest for the cholate sample. These data are in contradiction to the assertion that the intensity of the BWF mode may be taken as a direct measure of the SWNT aggregation state<sup>16,17</sup> and demonstrate that, in addition to the bundling effect on the BWF feature, other effects may be at play.

**Resonance Conditions.** For our analysis to be complete, we must consider the resonance conditions for Raman excitation as a function of surfactant and boron doping. As discussed above, Figure 2a shows that small shifts occur in the absorbance and PLE spectra for C-SWNTs dispersed in different surfactants.<sup>42</sup> While these shifts could possibly affect the resonance conditions for Raman excitation at 633 nm, Figure 3a demonstrates that the relative intensities of the RBM peaks are the same for the SWNT–cholate and SWNT–SDBS samples. Similarly, when comparing B-SWNTs to C-SWNTs, analysis of the second derivative of the absorbance spectra, the PLE spectra, and the RBM peaks suggests that the resonance conditions for these samples also do not change significantly. We also point to our results on SWNTs synthesized with a Nd:YAG laser and arc discharge. While these samples have a different mean diameter, which would imply a different distribution of tubes in resonance, we see exactly the same trends as those observed for the SWNTs synthesized with the alexandrite laser, shown here. These observations suggest that the large differences in the BWF intensity cannot be attributed to changes in the resonance conditions. Ultimately, the consideration of resonance conditions is inconsequential for the analysis of our data, since the main point is the unexpected observation of a BWF feature for isolated SWNTs.

**pH Dependence.** It has also been shown that solution pH can have a dramatic effect on the appearance and position of the BWF feature for surfactant-dispersed SWNTs.<sup>35</sup> In these experiments, a wider red-shifted BWF feature was observed for SDS-suspended SWNTs at high pH, while lowering the pH led to narrowing and blue-shifting of the feature.<sup>35</sup> It was also shown that acid protonation led to quenching of the  $E_{11}$  transitions because of valence band depletion due to oxidation. These same effects have been seen with the acidic polymer Nafion.<sup>33</sup> From Figure 2, it is evident that the SDS–SWNT sample studied here has lower intensity  $E_{11}$  transitions than the cholate and SDBS samples. This raises the possibility that the SDS surfactant produces an acidic environment at the surfactant–nanotube interface, which may lead to quenching of the BWF. To examine this possibility, we adjusted the pH of this SDS–SWNT solution in small increments up to pH = 10, taking Raman and absorbance spectra at each pH. As we increased the pH, we observed neither the development of a BWF feature in the Raman spectrum nor an increase in intensity of the  $E_{11}$  transitions in the absorbance spectrum. This suggests that the BWF is not simply quenched by acidic conditions for the SDS-dispersed SWNTs. Also, the pH values of the dispersions do not vary significantly as a function of surfactant. The pH values obtained for C-SWNTs dispersed in SDS, SDBS, and cholate were 7.6, 7.5, and 7.8, respectively, suggesting that macroscopic variations in pH are not responsible for the differences seen as a function of surfactant.

**Nanotube–Surfactant Interactions.** It is interesting to consider the observation that the intensity of the BWF feature scales with the dispersion yield of the different surfactants, that is, cholate > SDBS > SDS. We suggest that this scaling may

be attributable to the degree of charge polarization at the nanotube–surfactant interface. The electrostatic interaction between a localized charge on a surfactant molecule and a SWNT surface can be described as a polarization of charge at the site of the interaction. For example, an interaction with a surfactant species having a fixed negative charge may induce an offsetting positive charge distribution in the nanotube if the surfactant’s charged group is in proximity to the surface of the tube. A corresponding redistribution of charge on the nanotube results in an increase in electron density away from the interaction site. The net effect may be considered to be “charge injection”. Similarly, the interaction may be described as donating fractional electron density to the SWNT, resulting in what we term electronic polarization toward the nanotube surface. In contrast, interactions with a fixed positive charge cause partial electronic charge to be localized in the nanotube at the interaction site. Here, the net result is the removal of fractional electron density from the SWNTs because of electronic polarization away from the nanotube surface. We use the term electronic polarization because neither case involves a full charge transfer, and no bonds are formed or broken. Instead, the electronic charge of the SWNT is locally perturbed by interaction with the surfactant, resulting in a distributed negative charge ( $\delta^-$ ) on the SWNT if the surfactant contains electron-donating groups or a distributed positive charge ( $\delta^+$ ) if the surfactant contains electron-withdrawing groups.

To apply this argument to the observations made for our SWNT dispersions, we return to the observation made by Shim et al. of a large enhancement of the BWF mode for isolated SWNTs in contact with the electron-donating polymer polyethyleneimine (PEI).<sup>11</sup> Further, it has been suggested that the  $\pi$ – $\pi$  interactions between the benzene ring of SDBS and the SWNT surface contribute to its superior dispersion yields relative to SDS.<sup>41,44</sup> It has also been shown that the BWF feature is enhanced by the extended  $\pi$ – $\pi$  plasmon interactions associated with nanotube bundling.<sup>25–27</sup> Similar to the electronic effect of the SWNT/polymer composite,<sup>11</sup> the intertube van der Waals interaction gives rise to an enhanced BWF mode.

Thus, it also seems reasonable that  $\pi$ – $\pi$  interactions between the adsorbed benzene ring of the SDBS surfactant and the SWNT surface may lead to an enhancement of the BWF. Obviously, the degree of charge polarization should be lower for the SDBS–SWNT interaction, as the majority of the nanotube–surfactant interaction involves the aliphatic hydrocarbon chain as opposed to a nanotube–nanotube interaction in a bundle, which involves all  $\pi$ – $\pi$  interactions. However, the presence of a small BWF feature even for these highly debundled SWNTs suggests that even this small degree of  $\pi$ – $\pi$  interaction may contribute significantly to the development of this feature. Also, because of the  $\pi$ – $\pi$  interaction between the benzene ring of SDBS and the SWNT surface, the negative charge of the anionic sulfonate head group may be brought into close proximity to the nanotube surface, giving an even greater degree of electronic polarization at the SWNT surface.<sup>44</sup>

Tan and Resasco presented data that suggested naphthenic (saturated) rings provide better nanotube–surfactant interactions than aromatic rings, which explains the cholate molecule’s superior dispersion yields relative to SDBS and SDS.<sup>41</sup> The cholate molecule interacts with the nanotube surface by adopting a curved conformation, which places some of the hydroxyl groups near the nanotube surface.<sup>43</sup> The unpaired electrons of these hydroxyl groups should also serve to polarize negative charge on the nanotube surface to a greater extent than the benzene ring of SDBS. If we extend the hypothesis that the

BWF intensity is a function of the degree of electronic polarization, then the large increase in the electron density on the SWNT surface induced by the cholate–SWNT interaction would explain the large enhancement of the BWF feature for cholate relative to SDBS and SDS. For the SDS surfactant, only the aliphatic chain interacts with the SWNT surface, placing the anionic group farther away from the nanotube surface, and consequently the BWF feature is absent. These structural, packing, and electronic differences could explain the different relative intensities for the BWF feature in the different dispersions.

Finally, the results shown here qualitatively agree with the results recently reported for SWNT dispersions using DNA and SDS as surfactants.<sup>16,17</sup> These reports demonstrated the disappearance of the BWF feature for the surfactant-stabilized SWNT dispersions and a reappearance of the BWF when the SWNTs were allowed to aggregate in a film. Consistently, we also observe the lack of a BWF feature for SDS- and DNA-dispersed (data not shown) SWNTs. Interestingly, Karachevtsev et al. noted the interaction of electron-withdrawing groups on the DNA molecules with the SWNTs.<sup>17</sup> Thus, within the framework of our argument for the BWF sensitivity to electronic polarization, the lack of a BWF feature for a surfactant, such as DNA, that polarizes electron density away from the SWNT surface is entirely consistent.

**Boron Doping.** When comparing B-SWNTs to C-SWNTs in nonionic surfactants such as Triton X-100 (Figure 5b), the relative intensity of the BWF feature is higher for the C-SWNTs. At first inspection, this observation is in agreement with a greater degree of debundling for the B-SWNTs.<sup>25,26</sup> However, no PL is seen from either sample, suggesting that many bundles still exist and few nanotubes are fully isolated. For B-SWNTs in SDBS, we see a large enhancement for the BWF feature relative to C-SWNTs (Figure 5d, Table 1). Again, this enhanced BWF component would be surprising if the BWF intensity were solely dependent on the degree of aggregation, given the fact that the B-SWNTs show enhanced dispersion in the surfactant solutions with better resolved individual transitions in the absorbance spectrum and more intense PL. The enhanced dispersion, spectral resolution, and PL suggest a higher degree of debundling for the B-SWNTs relative to the undoped SWNTs.

The substitution of boron into the lattice introduces electron-deficient atoms into the SWNTs, lowering the Fermi level and making the nanotubes p-type.<sup>38</sup> The p-type B-SWNTs will thus have a small net positive charge ( $\delta^+$ ) delocalized over the nanotubes. Using the hypothesis that the intensity of the BWF is diminished by removing electron density from the m-SWNTs and is enhanced for increasing electron density, the reduced  $\pi$  electron density for the B-SWNTs explains the smaller BWF component in the Raman spectrum for the dry sample (Figure 5a). If, as suggested above, the surfactant–nanotube interaction involves electronic polarization from the surfactant to the SWNTs, this lowering of  $E_F$  may also explain the enhanced interaction with the surfactant molecules which contributes to the enhanced solubility.

The enhanced nanotube–surfactant interaction is an intriguing possibility, which may offer some insight into the differences observed in the Raman spectra between the SDBS-dispersed B-SWNTs and C-SWNTs. It is consistent to assert that the  $\delta^+$  charge of the p-type B-SWNT surface leads to an enhanced charge polarization toward the nanotube surface when the nanotubes interact with the anionic surfactants. The enhanced BWF component for the SDBS-dispersed B-SWNTs may then be related to the slight electron-donating capability of the

benzene ring or to the negative charge of the sulfonate head group which may interact with the nanotube surface.<sup>44</sup> These groups should interact more strongly with the boron-doped tubes because of the electron-accepting B sites and the overall p-type electronic character of the B-SWNTs.

Finally, we address the interesting observation that, while the cholate molecule provides the highest dispersion yields for C-SWNTs, B-SWNTs are not dispersed by this surfactant. While we do not have enough evidence at this point to conclusively explain this effect, we conjecture that the electron-accepting boron sites may interact strongly with the lone pairs on the hydroxyl groups of the cholate molecules. This interaction may serve to change the conformation of the cholate molecules<sup>43</sup> so that the surfactant layer is no longer able to produce stable micelles. This anomaly is very intriguing and warrants further study.

## Conclusion

In summary, we have explored the Raman spectra for laser-generated SWNTs dispersed in various surfactants to determine the sensitivity of the metallic BWF feature to bundling and nanotube–surfactant interactions. Disappearance of the BWF is seen for the SDS surfactant for these particular SWNTs, suggesting a dependence on bundling that is in agreement with several studies on isolated SWNTs. However, in some surfactants, a weak (SDBS) or even strong (cholate) BWF feature is still present, even for highly isolated SWNTs. Also, altering the SWNT electronic properties by substitutional doping with electron-deficient boron atoms leads to an enhancement of the BWF feature for SWNTs dispersed in SDBS. The general trend observed is an enhancement of the BWF feature for SWNT–surfactant interactions in which electron density is induced in the SWNT as a result of the surface dipole. This trend is in agreement with reports that demonstrate an electronic contribution to the BWF line shape that is enhanced by electron donation. These findings suggest that both bundling and electronic effects must be considered when analyzing the BWF feature for metallic SWNTs dispersed with surfactants or polymers and caution against using the presence or lack of such a feature as the sole measure of SWNT aggregation.

**Acknowledgment.** We would like to thank Joseph Luther and Matt Beard for assistance with peak fitting. This work was funded by the U.S. Department of Energy Office of Energy Efficiency and Renewable Energy Hydrogen Program and by the Office of Science, Basic Energy Sciences, Division of Materials Sciences and Engineering under subcontract DE-AC36-99GO10337 to NREL.

## References and Notes

- (1) Zhou, Y.; Gaur, A.; Hur, S.-H.; Kocabas, C.; Meitl, M. A.; Shim, M.; Rogers, J. A. *Nano Lett.* **2004**, *4*, 2031.
- (2) Artukovic, E.; Kaempgen, M.; Hecht, D. S.; Roth, S.; Gruner, G. *Nano Lett.* **2005**, *5*, 757.
- (3) Kong, J.; Franklin, N. R.; Zhou, C.; Chapline, M. G.; Peng, S.; Cho, K.; Dai, H. *Science* **2000**, *287*, 622.
- (4) Kazaoui, S.; Minami, N.; Nalini, B.; Kim, Y.; Hara, K. *J. Appl. Phys.* **2005**, *98*, 084314/1.
- (5) van de Lagemaat, J.; Barnes, T. M.; Rumbles, G.; Shaheen, S. E.; Coutts, T. J. *Appl. Phys. Lett.* **2006**, *88*, 233503.
- (6) Aguirre, C. M.; Auvray, S.; Pigeon, S.; Izquierdo, R.; Desjardins, P.; Martel, R. *Appl. Phys. Lett.* **2006**, *88*, 183104/1.
- (7) Dillon, A. C.; Heben, M. J. *Appl. Phys. A: Mater. Sci. Process.* **2001**, *72*, 133.
- (8) Collins, P. C.; Avouris, P. *Sci. Am.* **2000**, December, 62.
- (9) Iijima, S.; Ichihashi, T. *Nature* **1993**, *363*, 603.
- (10) Siddons, G. P.; Merchin, D.; Back, J. H.; Jeong, J. K.; Shim, M. *Nano Lett.* **2004**, *4*, 927.

- (11) Shim, M.; Ozel, T.; Gaur, A.; Wang, C. *J. Am. Chem. Soc.* **2006**, *128*, 7522.
- (12) Ago, H.; Shaffer, M. S. P.; Ginger, D. S.; Windle, A. H.; Friend, R. H. *Phys. Rev. B* **2000**, *61*, 2286.
- (13) Dresselhaus, M. S.; Dresselhaus, G.; Saito, R.; Jorio, A. *Phys. Rep.* **2005**, *409*, 47.
- (14) Dillon, A. C.; Yudasaka, M.; Dresselhaus, M. S. *J. Nanosci. Nanotechnol.* **2004**, *4*, 691.
- (15) Ericson, L. M.; Pehrsson, P. E. *J. Phys. Chem. B* **2005**, *109*, 20276.
- (16) Kawamoto, H.; Uchida, T.; Kojima, K.; Tachibana, M. *J. Appl. Phys.* **2006**, *99*, 094309.
- (17) Karachevtsev, V. A.; Glamazda, A. Y.; Dettlaff-Weglikowska, U.; Leontiev, V. S.; Mateichenko, P. V.; Roth, S.; Rao, A. M. *Carbon* **2006**, *44*, 1292.
- (18) Heller, D. A.; Barone, P. W.; Swanson, J. P.; Mayrhofer, R. M.; Strano, M. S. *J. Phys. Chem. B* **2004**, *108*, 6905.
- (19) Samsonidze, G. G.; Chou, S. G.; Santos, A. P.; Brar, V. W.; Dresselhaus, G.; Dresselhaus, M. S.; Selbst, A.; Swan, A. K.; Unlu, M. S.; Goldberg, B. B.; Chattopadhyay, D.; Kim, S. N.; Papadimitrakopoulos, F. *Appl. Phys. Lett.* **2004**, *85*, 1006.
- (20) Brar, V. W.; Samsonidze, G. G.; Santos, A. P.; Chou, S. G.; Chattopadhyay, D.; Kim, S. N.; Papadimitrakopoulos, F.; Zheng, M.; Jagota, A.; Onoa, G. B.; Swan, A. K.; Uenlue, M. S.; Goldberg, B. B.; Dresselhaus, G.; Dresselhaus, M. S. *J. Nanosci. Nanotechnol.* **2005**, *5*, 209.
- (21) Rao, A. M.; Eklund, P. C.; Bandow, S.; Thess, A.; Smalley, R. E. *Nature* **1998**, *388*, 257.
- (22) Brown, S. D. M.; Jorio, A.; Corio, P.; Dresselhaus, M. S.; Dresselhaus, G.; Saito, R.; Kneipp, K. *Phys. Rev. B* **2001**, *63*, 155414.
- (23) Klein, M. V. *Light Scattering in Solids I*; Springer-Verlag: Berlin, 1983.
- (24) Jorio, A.; Filho, A. J. S.; Dresselhaus, G.; Dresselhaus, M. S.; Swan, A. K.; Unlu, M. S.; Goldberg, B. B.; Pimenta, M. A.; Hafner, J. H.; Lieber, C. M.; Saito, R. *Phys. Rev. B* **2002**, *65*, 155412.
- (25) Paillet, M.; Poncharal, P.; Zahab, A.; Sauvajol, J. L.; Meyer, J. C.; Roth, S. *Phys. Rev. Lett.* **2005**, *94*, 237401.
- (26) Jiang, C.; Kempa, K.; Zhao, J.; Schlecht, U.; Kolb, U.; Basche, T.; Burghard, M.; Mews, A. *Phys. Rev. B* **2002**, *66*, 161404.
- (27) Kempa, K. *Phys. Rev. B* **2002**, *66*, 195406.
- (28) Bendiab, N.; Almairac, R.; Paillet, M.; Sauvajol, J. L. *Chem. Phys. Lett.* **2003**, *372*, 210.
- (29) Uchida, T.; Tachibana, M.; Kurita, S.; Kojima, K. *Chem. Phys. Lett.* **2004**, *400*, 341.
- (30) O'Connell, M. J.; Bachilo, S. M.; Huffman, C. B.; Moore, C. M.; Strano, M. S.; Haroz, E. H.; Rialon, K.; Boul, P. J.; Noon, W. H.; Kittrell, C.; Ma, J. P.; Hauge, R. H.; Weisman, R. B.; Smalley, R. E. *Science* **2002**, *297*, 593.
- (31) O'Connell, M. J.; Boul, P.; Ericson, L. M.; Huffman, C.; Wang, Y.; Haroz, E.; Kuper, C.; Tour, J.; Ausman, K. D.; Smalley, R. E. *Chem. Phys. Lett.* **2001**, *342*, 265.
- (32) Yu, Z.; Brus, L. E. *J. Phys. Chem. A* **2000**, *104*, 10995.
- (33) Engtrakul, C.; Davis, M. F.; Gennett, T.; Dillon, A. C.; Jones, K. M.; Heben, M. J. *J. Am. Chem. Soc.* **2005**, *127*, 17548.
- (34) Zhuo, W.; Vavro, J.; Nemes, N. M.; Fischer, J. E.; Borondics, F.; Kamaras, K.; Tanner, D. B. *Phys. Rev. B* **2005**, *71*, 205423.
- (35) Strano, M. S.; Huffman, C. B.; Moore, C. M.; O'Connell, M. J.; Haroz, E. H.; Hubbard, J.; Miller, M.; Rialon, K.; Kittrell, C.; Ramesh, S.; Hauge, R. H.; Smalley, R. E. *J. Phys. Chem. B* **2003**, *107*, 6979.
- (36) Ye, J. T.; Li, Z. M.; Tang, Z. K.; Saito, R. *Phys. Rev. B* **2003**, *67*, 113404.
- (37) Chen, G.; Furtado, C. A.; Kim, U. J.; Eklund, P. C. *Phys. Rev. B* **2005**, *72*, 155406.
- (38) Blackburn, J. B.; Yan, Y.; Jones, K. M.; Gennett, T.; Engtrakul, C.; Dillon, A. C.; Heben, M. J. *Chem. Mater.* **2006**, *18*, 2558.
- (39) Dillon, A. C.; Parilla, P. A.; Alleman, J. L.; Gennett, T.; Jones, K. M.; Heben, M. J. *Chem. Phys. Lett.* **2005**, *401*, 522.
- (40) Dillon, A. C.; Parilla, P. A.; Alleman, J. L.; Perkins, J. D.; Heben, M. J. *Chem. Phys. Lett.* **2000**, *316*, 13.
- (41) Tan, Y.; Resasco, D. E. *J. Phys. Chem. B* **2005**, *109*, 14454.
- (42) Moore, V. C.; Strano, M. S.; Haroz, E. H.; Hauge, R. H.; Smalley, R. E. *Nano Lett.* **2003**, *3*, 1379.
- (43) Usrey, M. L.; Lippman, E. S.; Strano, M. S. *J. Am. Chem. Soc.* **2005**, *127*, 16129.
- (44) Islam, M. F.; Rojas, E.; Bergey, D. M.; Johnson, A. T.; Yodh, A. G. *Nano Lett.* **2003**, *3*, 269.
- (45) Izard, N.; Riehl, D.; Anglaret, E. *Phys. Rev. B* **2005**, *71*, 195417.
- (46) Fantini, C.; Jorio, A.; Souza, M.; Strano, M. S.; Dresselhaus, M. S.; Pimenta, M. A. *Phys. Rev. Lett.* **2004**, *93*, 147406.
- (47) McGuire, K.; Gothard, N.; Gai, P. L.; Dresselhaus, M. S.; Sumanasekera, G.; Rao, A. M. *Carbon* **2005**, *43*, 219.
- (48) The enhanced intensity for the RBM modes is seen for all B-SWNT samples, in both dry and solvated forms. This implies that the enhanced intensity is intrinsic to the B-SWNTs themselves and does not result from SWNT-surfactant interactions. Our assertion that the enhancement is due to an increase in the absorbance cross section is supported by differences in the absorbance spectra for B-SWNTs and C-SWNTs when the spectra are normalized to the rising background that peaks in the ultraviolet. When normalized in this manner, the integrated area underneath each grouping of van Hove singularities is always significantly greater for the B-SWNTs than for the C-SWNTs. We are in the process of carefully quantifying the absorbance cross sections for each type of SWNT and plan to report on this effect in the near future.
- (49) Brown, C. M.; Corio, P.; Marucci, A.; Dresselhaus, M. S.; Pimenta, M. A.; Kneipp, K. *Phys. Rev. B* **2000**, *61*, R5137.
- (50) Jorio, A.; Dresselhaus, G.; Dresselhaus, M. S.; Souza, M.; Dantas, M. S. S.; Pimenta, M. A.; Rao, A. M.; Saito, R.; Liu, C.; Cheng, H. M. *Phys. Rev. Lett.* **2000**, *85*, 2617.